Characterization of model automotive exhaust catalysts: Pd on Zr-rich ceria–zirconia supports

G.W. Graham, H.-W. Jen, R.W. McCabe, A.M. Straccia and L.P. Haack

Ford Research Laboratory, MD3179/SRL, PO Box 2053, Dearborn, MI 48121, USA

Received 17 March 2000; accepted 19 May 2000

Model Pd automotive three-way catalysts were prepared with high-surface-area Zr-rich ceria–zirconia powders as support materials, aged for 12 h at 1050 °C under redox conditions simulating automotive exhaust gases, and characterized by a combination of techniques including oxygen storage capacity (OSC) measurements. Differences in OSC amongst aged catalysts made with materials of similar ceria–zirconia compositions, but produced by different processes, were weakly correlated with differences in support surface area. Evidence of encapsulation of Pd particles was found in most of the aged catalysts. The promotional effect of zirconia on ceria reducibility, well known from previous temperature-programmed H_2 reduction studies, was apparent in Ce 3d core-level spectra from X-ray photoelectron spectroscopy measurements, which showed that both X-ray-induced and H_2 reduction become increasingly facile with increasing zirconia content. A slight Ce enrichment at the surface of the fresh catalysts made with the more Zr-rich powders was found to increase upon aging.

Keywords: palladium, ceria–zirconia, oxygen storage, automotive exhaust catalyst

1. Introduction

High-surface-area ceria–zirconia is widely used as a support for precious metals in automotive three-way catalysts, where its introduction during the middle of the 1990's led to Pd-based catalysts of exceptional thermal stability [1–4]. Although materials spanning a wide composition range are of interest, most attention has been given to Ce-rich material, typically containing about 70 wt% ceria, since it tends to have the largest oxygen storage capacity (OSC) [5]. In the present study, we examine model Pd catalysts made with Zr-rich ceria–zirconias and contrast some of their properties with those of catalysts made with Ce-rich materials [6].

2. Experimental

Model catalysts containing 2 wt% Pd were prepared by impregnation of various commercial-grade ceria–zirconias with an aqueous solution of Pd nitrate to incipient wetness, followed by drying for 12 h at 55 °C and calcination at 600 °C for an additional 12 h in a standard muffle furnace. The ceria–zirconia compositions and designations of the catalysts made with them are contained in table 1.

Catalysts were aged under a laboratory redox cycle designed to simulate air–fuel variations of automotive exhaust [6]. Redox aging was carried out for 12 h at 1050 °C (and occasionally at 1150 °C) in flowing gases in a tube furnace containing a 3 cm o.d. quartz tube. The powder samples were distributed as thin layers in quartz boats inserted into the tube. The gas mixture contained 1 mol% CO/H_2 ($[CO]/[H_2] = 3/1$), alternating every 10 min with 0.5 mol% O_2, together with 0.002 mol% SO_2, 10 mol% H_2O, and balance N_2 (total flow rate at STP of 5000 cm^3/min). The redox aging ended with the oxidizing portion of the cycle, followed by 30 min of natural cooling in flowing N_2 to about 500 °C. The N_2 flow was then stopped and the sample was cooled to room temperature with the outlet of the tube open to air.

The specific surface areas of the powders were determined by the BET method with a Micromeritics Gemini 2360 surface area analyzer. Samples were degassed under flowing inert gas at 250 °C for at least 30 min before measurement. The estimated error in the measurement is 5% (relative).

Powder X-ray diffraction (XRD) data were obtained with a Scintag X1 diffractometer, in θ–θ orientation, using Cu K_α radiation. The samples were held in a cylindrical cavity, 9 mm in diameter and 0.5 mm deep, cut into the surface of a zero-background quartz plate.

Oxygen storage measurements were carried out in a flow reactor system, designed for powder samples, equipped with solenoid valves for rapid introduction of step pulses

Table 1
Designations, nominal ceria–zirconia compositions, and specific surface areas.

Designation	Composition (wt%)		Surface area (m^2/g)	
	CeO_2	ZrO_2	Fresh	Aged
Pd/ZC1	20	80	50	7
Pd/ZC2	20.1	79.9	80	2
Pd/ZC3	21.2	78.8	77	12
Pd/ZC4	19.4	80.6	61	6
Pd/ZC5	40	60	69	4
Pd/ZC6	50	50	70	3
Pd/ZC7	50	50	86	9

of CO and O_2 [6]. Samples were prepared by pressing the powders into disks, then breaking the disks into small pieces. The pieces were loaded into a 0.4 cm i.d. quartz U-tube reactor, located within a furnace. A total gas flow rate of 500 cm^3/min (STP) was employed through a catalyst bed typically 2.2 cm in length, yielding a pressure drop of about 3.5 kPa (∼0.5 psi) at room temperature. Prior to an OSC measurement, the sample was first heated in 2.5% O_2/He at 500 °C for at least 20 min. The sample was then exposed to alternating 2.5% O_2 and 5% CO pulses (both in He carrier) at the desired test temperature. Most of the OSC data reported here involved five sequences of 10 s pulses with 10 s He pulses interspersed to ensure complete flushing of gas phase species between the O_2 and CO pulses (a few experiments were carried out with 50 s pulses of CO and O_2 with 10 s of He in-between). Ar was injected along with the CO pulse and was used as an internal standard for quantification of gas concentrations. A UTI 100C quadrupole mass spectrometer was used to monitor CO (mass 28), O_2 (mass 32), Ar (mass 40), and CO_2 (mass 44) at 0.2 s intervals during each measurement. Corrections were made to the mass 28 and 32 signals due to cracking of CO_2. OSC was quantified in terms of micromoles of oxygen atoms per gram of catalyst (μmol O/g) by comparing integrated amounts of CO in the pulses entering and exiting the reactor. Close agreement was obtained between oxygen uptakes calculated from consumption of CO and those calculated from either production of CO_2 or consumption of O_2 (during subsequent re-oxidation of the catalyst).

X-ray photoelectron spectroscopy (XPS) measurements were performed with a Kratos Axis 165 spectrometer and coupled reactor, which allowed for sample treatment followed by analysis without exposure to air. Samples were prepared by pressing the powders into pellets. In order to accelerate outgassing and remove C from the surface, samples were heated at 450 °C for 2 h in flowing O_2 before performing the first set of XPS measurements. A second set of measurements was performed subsequently, following a similar treatment in flowing H_2. Each set of measurements included a survey spectrum and the Ce 3d, Zr 3d, and Ce 4d core-level spectra, which were analyzed following standard procedures using Kratos-supplied software.

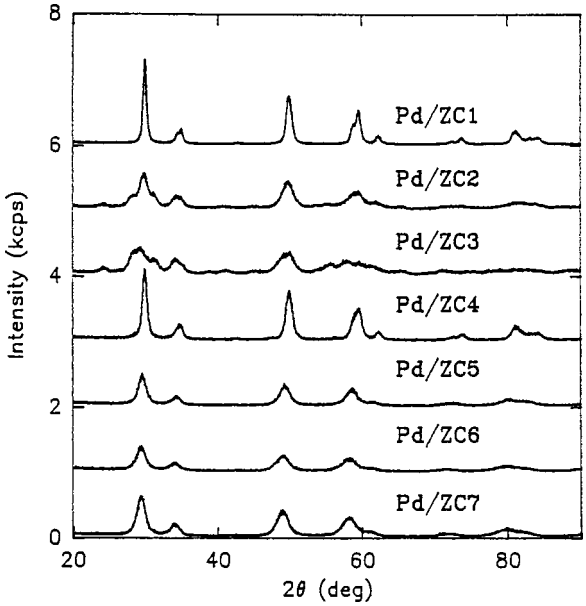

Figure 1. XRD patterns of fresh catalysts.

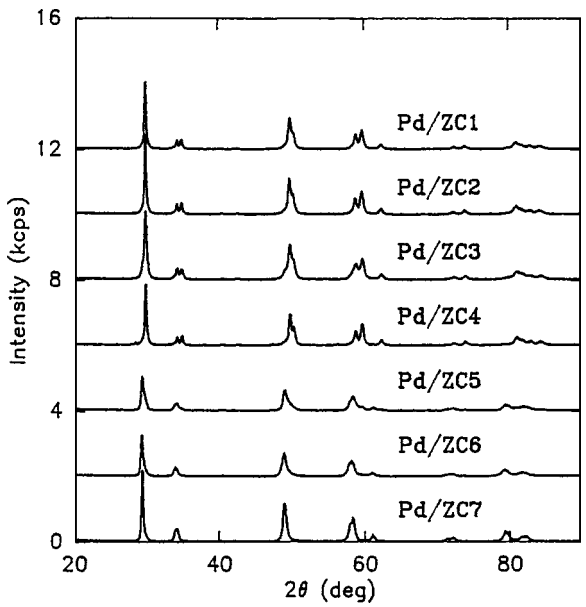

Figure 2. XRD patterns of aged (1050 °C redox for 12 h) catalysts.

3. Results

The specific surface areas of both fresh and aged catalysts are listed in table 1. Aside from the decrease upon aging, there are no clear trends, e.g., with variation in composition. Within the series Pd/ZC1–Pd/ZC4, each of which contains approximately 80 wt% zirconia, surface areas after aging vary by a factor of five, whereas fresh surface areas are more nearly comparable. A similar difference in stability exists between Pd/ZC6 and Pd/ZC7, each of which contains 50 wt% zirconia.

Powder XRD patterns of the fresh catalysts are shown in figure 1. The patterns of Pd/ZC1 and Pd/ZC4 resemble that of tetragonal ZrO_2 [7], distinguishable from the cubic fluorite-type structure by the splitting of certain peaks, like the ones near 59° and 73°. The patterns of Pd/ZC2 and Pd/ZC3 resemble a mixture of tetragonal (or cubic) and monoclinic ZrO_2 [7]. Dissolution of increasing amounts of ceria into zirconia causes all the peaks of the tetragonal structure to shift toward lower angles, as can be seen from a close comparison of the patterns of Pd/ZC4, Pd/ZC5, and Pd/ZC6. The patterns of Pd/ZC5–Pd/ZC7 resemble that of cubic ZrO_2 (or CeO_2) [7].

The XRD patterns shown in figure 2 were obtained from the aged catalysts. Compared with the patterns of the fresh catalysts, the peaks are narrower, due to sintering, and closely spaced peaks are more clearly resolved. The mon-

Table 2
XRD results: phase compositions, cell parameters, and %Pd encapsulated.

Designation	Phase[a] (cell parameters (nm))[b]		%Pd encapsulated
	Fresh	Aged	(aged)
Pd/ZC1	t	t (0.512, 0.522)	∼5
Pd/ZC2	t(/c), m	t (0.512, 0.522)	∼20
Pd/ZC3	t(/c), m	t (0.512, 0.522)	∼7
Pd/ZC4	t	t (0.512, 0.522)	15–20
Pd/ZC5	c	t (0.513, −), t′ (−, 0.527)	15–25
Pd/ZC6	c	t′ (0.524, −)	20–25
Pd/ZC7	c	t′ (0.524, 0.528)	∼0

[a] m – monoclinic (ZrO_2), t, t′ – tetragonal, c – cubic.
[b] (a, c) of double tetragonal cell.

oclinic ZrO_2 has disappeared from Pd/ZC2 and Pd/ZC3, making the patterns of the series Pd/ZC1–Pd/ZC4 nearly identical. In fact, cell parameters (a, c) deduced from the positions of the peaks corresponding to (200) and (002) reflections of the double tetragonal cell, listed in table 2, are the same for all four aged catalysts. The patterns of Pd/ZC6 and Pd/ZC7 are now also seen to be tetragonal rather than cubic, but their cell parameters are larger than those of Pd/ZC1–Pd/ZC4, as would be expected due to their larger Ce content. Further, their c/a ratio is closer to one, leading to the distinction in labeling of the two tetragonal phases, t and t′, in table 2. The pattern of Pd/ZC5 appears to contain a mixture of these two tetragonal phases. Although this variation in phase with composition has been previously reported [8], the measured cell parameters of phase t in the present case are smaller (by 0.002 nm) than expected for the nominal composition (and thus typical of a more Zr-rich material), implying that the materials in these aged catalysts are not homogeneous.

In fact, close inspection of the two largest peaks in each of the patterns from Pd/ZC1–Pd/ZC4 in figure 2, especially Pd/ZC3, reveals a weak low-angle tail or shoulder, suggesting the presence of another, minor phase. Aging at higher temperature, 1150 °C, leads to the clear development of these peaks, as shown by the XRD pattern of Pd/ZC1 in figure 3. Here, after aging at 1150 °C, the cell parameters of the original phase, t, have decreased slightly to (0.511,0.521), and the peaks corresponding to the new phase appear to match those of the more Ce-rich phase, t′. Additionally, weak peaks corresponding to monoclinic ZrO_2 appear. Such thermally induced phase separation also occurs in Ce-rich ceria–zirconia, but higher temperatures (by at least 100 °C in the case of 70 wt% CeO_2–30 wt% ZrO_2) are required. In general, phase separation is observed at lower temperatures when aging is performed in air, e.g., [6].

The XRD patterns shown in figure 4, also obtained from the catalysts aged at 1050 °C, but with a higher signal-to-noise ratio than the patterns in figure 2, span a narrow range of angles around the (111) peak of Pd, normally centered at 40.1°. The additional peak near 40.5°, present in most of the patterns, is thought to arise from encapsulated Pd particles that are under a compressive stress applied by the

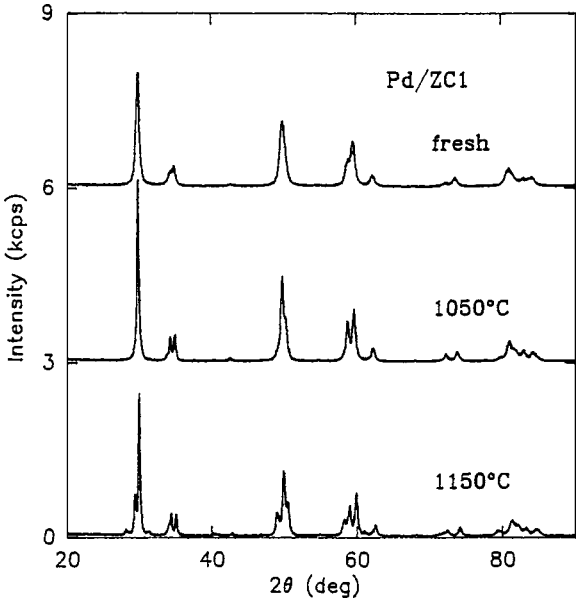

Figure 3. XRD patterns of Pd/ZC1 showing progression of sintering and phase separation with increasing aging temperature.

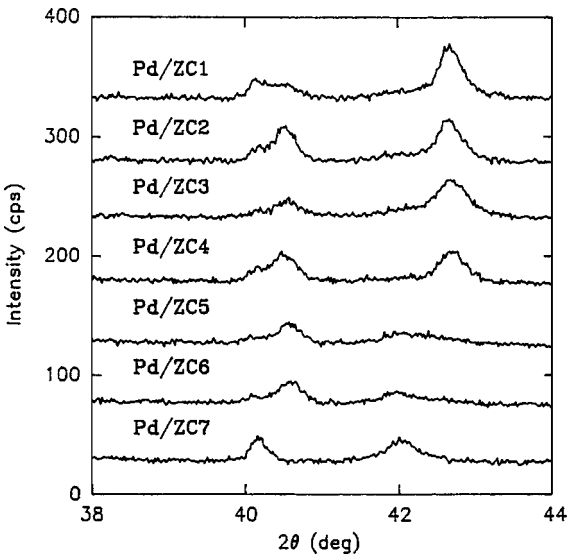

Figure 4. XRD patterns of aged catalysts over narrow range of 2θ spanning Pd(111) diffraction peak.

ceria–zirconia [9]. The other structure comes from ceria–zirconia (producing a peak near 42.6° in Pd/ZC1–Pd/ZC4 but closer to 42° in the more Ce-rich compositions) and PdO (producing a broad, weak peak at 41.9°). The encapsulated Pd can be observed more clearly by heating the aged sample in air at 700 °C for 2 h, in order to oxidize any metallic Pd that is not encapsulated, and the encapsulated fraction can then be deduced by comparison of its peak intensity with that of the reduced sample, where all PdO has reverted to Pd and the stress on encapsulated Pd particles has been removed. These steps are illustrated for Pd/ZC1 in figure 5, which also shows the pattern from aged ZC1 with no Pd in order to demonstrate the absence of any other structure in the background. In this case, approximately 5%

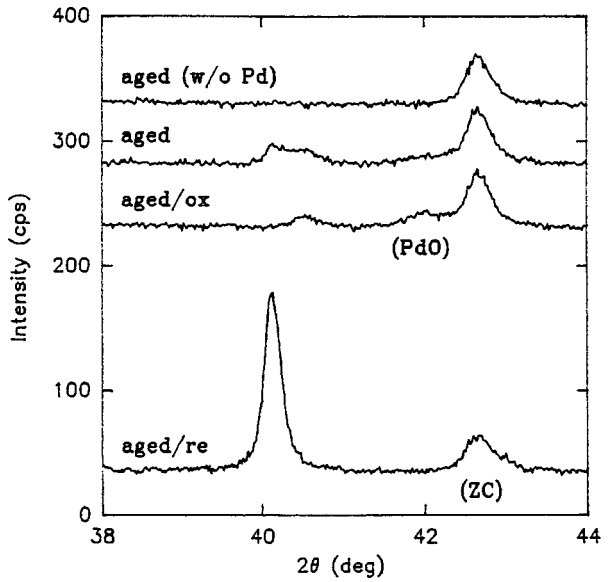

Figure 5. XRD patterns of Pd/ZC1 showing separated structure due to diffraction from free and encapsulated Pd particles, PdO, and ceria–zirconia (ZC). The labels, aged/ox and aged/re, refer to aged catalysts which have subsequently been heated in air at 700 °C for 2 h or heated in 0.5% H_2 at 500 °C for 0.5 h, respectively.

Table 3
Oxygen storage capacities derived from fifth pulse sequence after aging.

Designation	Oxygen storage capacity (μmol O/g)		
	350 °C	500 °C	700 °C
Pd/ZC1	160	160	390
Pd/ZC2	20	110	270
Pd/ZC3	220	260	400
Pd/ZC4	50	140	260
Pd/ZC5	150	400	670
Pd/ZC6	150	420	730
Pd/ZC7	470	570	970

of the Pd appears to be encapsulated. Estimates of the encapsulated fraction of Pd for all the aged catalysts are listed in table 2. Generally, these values tend to be relatively high in catalysts in which the surface area is relatively low, as noted previously [9]. Application of the Scherrer relation to the (111) peak of Pd indicates that the Pd particles are about 40 nm in diameter.

Results of the OSC measurements are listed in table 3. The order in which the measurements were performed was 500 °C, then 700 °C, and finally 350 °C. While changing temperature, the catalyst was continuously exposed to 2.5% O_2/He. The values listed were deduced from the fifth of the multi-pulse sequences and are taken as characteristic of steady state. (The first pulse sequence typically yielded between 60 and 100 μmol O/g more OSC than the fifth at both 350 and 500 °C, but there was little difference between them at 700 °C.) Within each of the two series of catalysts having similar compositions, the ordering of OSC for all of the temperatures basically follows that of specific surface area. The values for the catalyst with the highest OSC from each series are listed in table 4 together with those

Table 4
Steady-state oxygen storage capacities of aged catalysts.[a]

Designation	CeO_2	Oxygen storage capacity (μmol O/g)		
	(wt%)	350 °C	500 °C	700 °C
Pd/ZC3	21.2	220	260	400
Pd/ZC5	40	150	400	670
Pd/ZC7	50	470	570	970
Pd/CZ3[b,c]	70.1	630	810	1070
Pd/CZ1[d,c]	89.6	300	460	620
Pd/C2[c]	100	20	30	80

[a] Fifth short pulse for Pd/ZC3,5,7 and Pd/CZ3, long pulse for others.
[b] 70.1 wt% ceria–29.9 wt% zirconia.
[c] Catalysts described in [6].
[d] 89.6 wt% ceria–10.4 wt% zirconia.

for comparable catalysts made with Ce-rich ceria–zirconias (Pd/CZ1 and Pd/CZ3) and pure ceria (Pd/C2) that were the subject of an earlier investigation [6]. These results provide confirmation that the maximum OSC, on a weight basis, occurs near the center of the Ce-rich side of the composition range.

The two catalysts made with the Ce-rich ceria–zirconias, listed in table 4, were also examined by XPS, together with a subset of the catalysts made with the Zr-rich ceria–zirconias. Figure 6 shows the Ce 3d spectra from the fresh catalysts after both the oxidative and reductive treatments. The spectrum from Pd/CZ1 after the oxidative treatment is characteristic of Ce^{4+}, while that after the reductive treatment is characteristic of a mixture of Ce^{4+} and Ce^{3+} [10]. As the Zr content increases, the relative amount of Ce^{3+} increases, both after the oxidative and reductive treatments. In the case of the oxidative treatment, Ce^{3+} is not expected to be stable, and its presence is attributed to X-ray-induced reduction of Ce^{4+} to Ce^{3+}, e.g., [11], a process that becomes more facile in the more Zr-rich catalysts. The temporal dependence of this effect is illustrated for the fresh Pd/ZC5 catalyst in figure 7, which shows Ce 3d spectra (acquired over a period of 15 min each) taken at 30 min intervals. Qualitatively similar behavior was found for the aged catalysts.

The H_2 reductive treatment is more effective than X-rays for reducing Ce^{4+} to Ce^{3+} in all the catalysts, however, according to figure 6. The percentage of Ce present as Ce^{3+} after this treatment, deduced by deconvolution of the Ce $3d_{5/2}$ spectra into Ce^{3+} and Ce^{4+} contributions using computer fits to spectra from appropriate reference compounds, is listed in table 5. The increasing percentage of Ce^{3+} in cerium–zirconium mixed oxides with increasing Zr content, also observed in temperature-programmed H_2 reduction measurements [12], coupled with the decreasing Ce content, leads to a broad maximum in overall reducibility for intermediate compositions.

Quantification of surface composition was performed using the XPS survey spectra. Figure 8 presents the results, expressed in terms of wt% CeO_2, for the fresh catalysts, where either the Ce 3d or 4d core levels were used for obtaining the surface CeO_2 concentration, and the Zr 3d core level was used for obtaining the surface ZrO_2 concen-

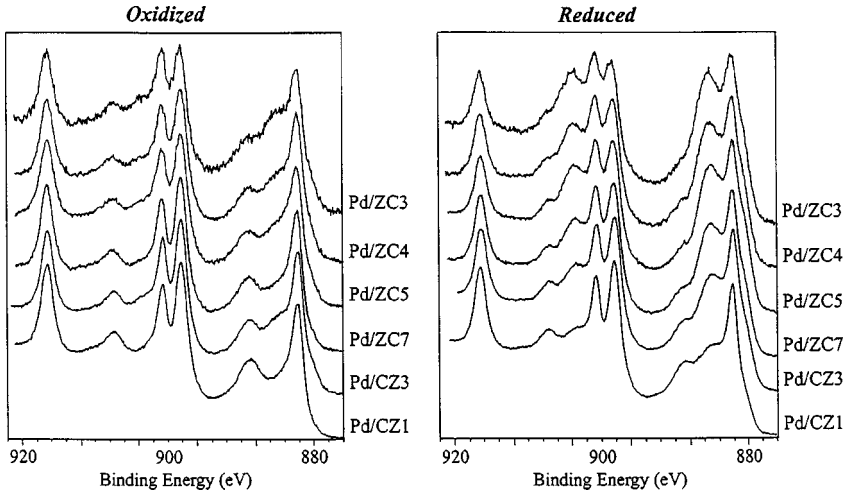

Figure 6. Ce 3d core-level spectra of fresh catalysts subjected to oxidative and reductive treatments.

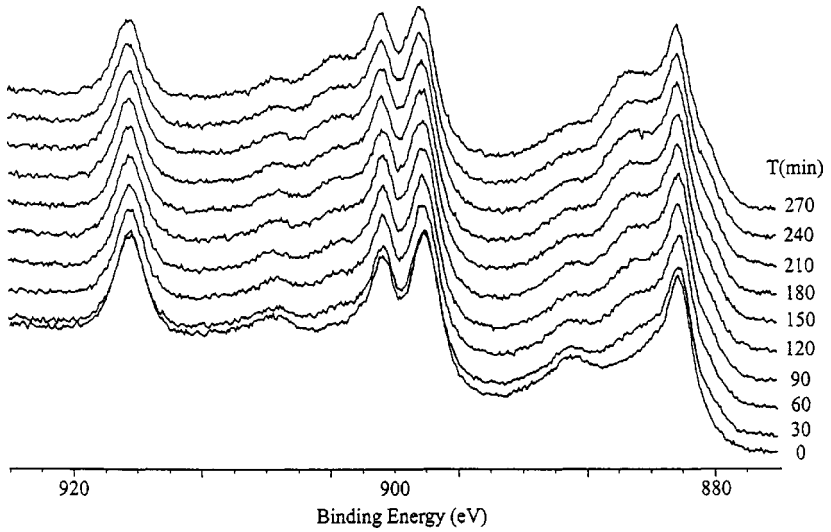

Figure 7. Evolution of Ce 3d spectrum of fresh Pd/ZC5 upon exposure to X-rays.

Table 5
Percentage of Ce as Ce^{3+}, according to XPS, after the reductive treatment.

Designation	CeO_2 (wt%)	Fresh	Aged
Pd/ZC3	21.1	71	73
Pd/ZC4	19.4	68	67
Pd/ZC5	40	69	55
Pd/ZC7	50	60	55
Pd/CZ3[a]	70.1	49	39
Pd/CZ1[b]	89.6	33	30

[a] 70.1 wt% ceria–29.9 wt% zirconia [6].
[b] 89.6 wt% ceria–10.4 wt% zirconia [6].

tration. While the correlation between surface and nominal bulk compositions is good, there is a hint of surface enrichment in Ce for the most Zr-rich catalysts. The difference between the Ce 3d and 4d results for these catalysts is consistent with such Ce surface enrichment since the Ce 3d photoelectrons originate from closer to the surface than

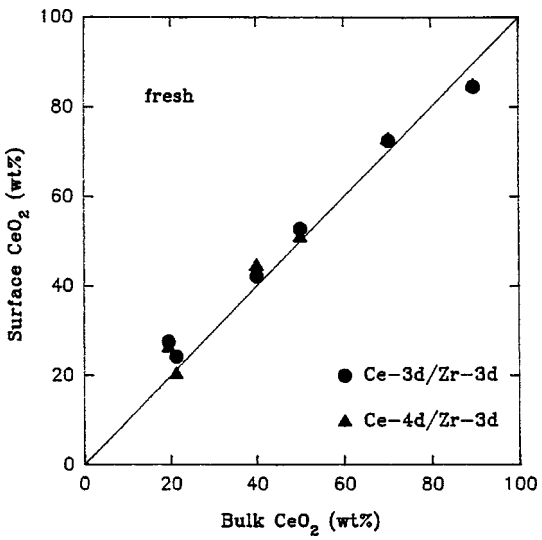

Figure 8. Surface composition of fresh catalysts derived from XPS measurements.

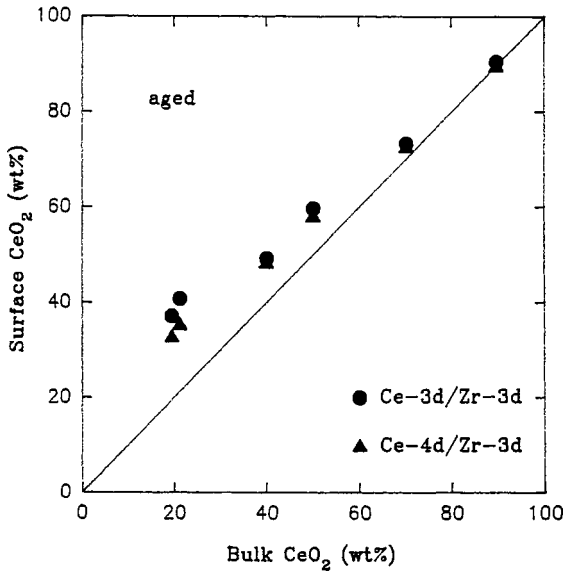

Figure 9. Surface composition of aged catalysts derived from XPS measurements.

the Ce 4d electrons due to their shorter inelastic mean-free path. Further, the surface enrichment in Ce for the more Zr-rich catalysts appears to have increased after aging, as shown by figure 9. Although an earlier study did not observe this effect [13], it would seem to be reasonable in view of the incipient phase separation, where the more Ce-rich minor phase, which has the larger cell volume, could possibly reduce strain energy if it formed preferentially at the surface.

Finally, a binding energy shift of about 0.5 eV in the Zr 3d levels of the Ce-rich mixed oxides relative to those in pure zirconia was observed. This agrees with measurements from $Ce_{1-x}Zr_xO_2$ epitaxial films, where the shift was attributed to the "alloy" effect [14].

4. Discussion

The results of this study complement those of an earlier one in which model Pd automotive catalysts were made with high-surface-area Ce-rich ceria–zirconias, aged, and characterized [6]. Similarities and differences are summarized below:

- Specific surface areas of catalysts made with both Zr- and Ce-rich materials were comparable, spanning the range 50–100 m^2/g when fresh and 2–10 m^2/g when aged.
- Both Zr- and Ce-rich ceria–zirconias can be made in the form of single-phase solid solutions, but upon aging, Zr-rich materials phase separated at lower temperature than Ce-rich materials. The crystal structures of the solid solutions are also different, Zr-rich being tetragonal, Ce-rich being cubic.
- Sintering of Pd upon aging was comparable in all catalysts. The extent of Pd particle encapsulation was no greater, in some of the cases, for the Zr-rich ceria–zirconias than for the Ce-rich ceria–zirconias.
- The fraction of Ce that becomes Ce^{3+} upon reduction was larger on the Zr-rich side of the composition range, but OSC reached a maximum value for catalysts made with compositions near the middle of the Ce-rich side.
- Surface segregation of Ce was observed upon aging of catalysts made with Zr-rich ceria–zirconia, whereas none was found in catalysts made with Ce-rich material.

The previous study also employed another characterization technique, temperature-programmed reduction with H_2, which revealed a new feature in aged catalysts made with ceria–zirconia, relative to ceria, related to Pd-assisted reduction of the ceria–zirconia bulk. Although not shown, similar results have been obtained for Pd catalysts made with Zr-rich ceria–zirconias [15].

A particularly interesting aspect of the previous study was the difference in OSC amongst catalysts made with a series of ceria–zirconias having the same composition, 70 wt% CeO_2–30 wt% ZrO_2, and nearly identical physical characteristics, but produced by different processes. In the present study, the catalysts made with the series of ceria–zirconias having a composition of 20 wt% CeO_2–80 wt% ZrO_2 were not as similar, and after aging, the differences in OSC were weakly correlated with differences in specific surface area.

Aside from any differences associated with the preparation process, it is clear that ceria–zirconia having a composition of 70 wt% CeO_2–30 wt% ZrO_2 provides the largest OSC, and yet there may be situations that favor the use of other compositions. Consider, for example, maintenance of stable OSC under extremely high-temperature conditions, sufficient to cause phase separation. Although the temperature required would likely be somewhat higher for a Ce- than a Zr-rich material, the effect of phase separation on a material with maximum OSC would be to produce multiple phases, each possessing a lower OSC, the sum of which would be less than the initial value. Phase separation in a Zr-rich material, on the other hand, would likely produce one phase (out of at least two) with a higher OSC than the initial value, and overall OSC might not change much at all.

Another factor, not considered in these studies, that could influence the relative performance of different ceria–zirconias, is the effect of sulfur poisoning. Preliminary results in our laboratory suggest that exposure to SO_2 may produce a much larger decrease in OSC of Pd catalysts made with Ce- than Zr-rich ceria–zirconias. Further, different relationships may exist for Pt and Rh, the other precious metals commonly used in automotive exhaust catalysts, when supported on ceria–zirconia [9].

References

[1] G.J. Bartley et al., Paper No. 930076, Society of Automotive Engineers, Warrendale, PA (1993).

[2] B.H. Engler et al., Paper No. 930738, Society of Automotive Engineers, Warrendale, PA (1993).
[3] J.C. Summers, J.J. White and W.B. Williamson, Paper No. 890794, Society of Automotive Engineers, Warrendale, PA (1989).
[4] J.S. Hepburn et al., Paper No. 941058, Society of Automotive Engineers, Warrendale, PA (1994).
[5] J.-P. Cuif et al., Paper No. 970463, Society of Automotive Engineers, Warrendale, PA (1997).
[6] H.-W. Jen, G.W. Graham, W. Chun, R.W. McCabe, J.-P. Cuif, S.E. Deutsch and O. Touret, Catal. Today 50 (1999) 309.
[7] JCPDS files: 17-923 (tetragonal ZrO_2), 37-1484 (monoclinic ZrO_2), 34-394 (CeO_2).
[8] S. Meriani and G. Spinolo, Powder Diffraction 2 (1987) 255.
[9] G.W. Graham, H.-W. Jen, W. Chun and R.W. McCabe, J. Catal. 182 (1999) 228.
[10] M. Shelef, L.P. Haack, R.E. Soltis, J.E. de Vries and E.M. Logothetis, J. Catal. 137 (1992) 114.
[11] P.W. Park and J.S. Ledford, Langmuir 12 (1996) 1794.
[12] A. Trovarelli, F. Zamar, J. Llorca, C. de Leitenburg, G. Dolcetti and J.T. Kiss, J. Catal. 169 (1997) 490.
[13] A. Galtayries, R. Sporken, J. Riga, G. Blanchard and R. Caudano, J. Electron Spectrosc. Relat. Phenom. 88–91 (1998) 951.
[14] Y. Gao, G.S. Herman, S. Thevuthasan, C.H.F. Peden and S.A. Chambers, J. Vac. Sci. Technol. A 17 (1999) 961.
[15] P. Andersen, private communication.